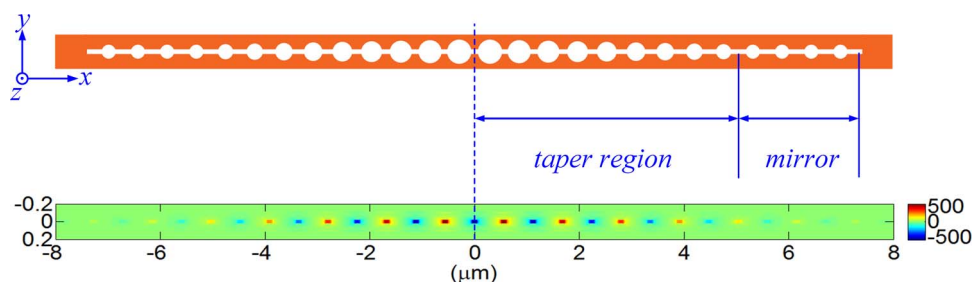# Ultrahigh-*Q* and Low-Mode-Volume Parabolic Radius-Modulated Single Photonic Crystal Slot Nanobeam Cavity for High-Sensitivity Refractive Index Sensing

Daquan Yang
Pan Zhang
Huiping Tian
Yuefeng Ji
Qimin Quan

Ultrahigh-Q and Low-Mode-Volume Parabolic Radius-Modulated Single Photonic Crystal Slot Nanobeam Cavity for High-Sensitivity Refractive Index Sensing

Daquan Yang,[1] **Pan Zhang,**[1] **Huiping Tian,**[1] **Yuefeng Ji,**[1] **and Qimin Quan**[2]

[1]State Key Laboratory of Information Photonics and Optical Communications, School of Information and Communication Engineering, Beijing University of Posts and Telecommunications, Beijing 100876, China
[2]Rowland Institute at Harvard University, Cambridge, MA 02142 USA

Abstract: We present a novel optical sensor based on the design of ultrahigh-Q and low-mode-volume 1-D single photonic crystal (PhC) slot nanobeam cavity (SNC) in which the air-hole radius is parabolically tapered. The performance of the device is investigated theoretically. In order to achieve high Q-factor and high sensitivity simultaneously, the slot geometry is exploited to make the optical field strongly localized inside the low index region and overlaps sufficiently with the analytes. With the three-dimensional finite-difference time-domain (3D-FDTD) method, we demonstrate that the proposed single 1-D PhC-SNC sensor device possess an ultrahigh sensitivity (S) up to $\sim$900 nm/RIU (refractive index unit, RIU) and a high Q-factor in air up to $> 10^7$ at the telecom wavelength range. The optimized figure of merit is $> 10^7$. In addition, an ultrasmall mode volume of $V_m \sim 0.01 \ (\lambda/n_{air})^3$ has been achieved, which is more than three orders of magnitude smaller than our previous works [*Appl. Phys. Lett.* 105, 063118 (2014)] and, thus, is potentially an ideal platform for realizing ultracompact laboratory-on-a-chip applications with dense arrays of functionalized spots for multiplexed gas sensing.

Index Terms: Photonic crystals, sensors, nanocavities, integrated nanophotonic, three-dimensional finite-difference time-domain (3D-FDTD).

1. Introduction

Over the past few years, compared with 2-D photonic crystal (PhC) cavities [1], [2], 1-D photonic crystal nanobeam cavities have emerged as an advantageous platform for on-chip optical technology, owing to their attractive properties such as confining light in a small volume, convenient integration with waveguides, compact foot print, and ultra-high Q-factors [3]–[13]. One-dimensional PhC nanobeam cavities have been proposed and demonstrated for various applications, e.g., quantum optics [14],[15], non-linear optics [16], [17], optomechanics [18]–[20], optical trapping [21], [22], light modulators [23], [24], lasers [25], [26], filters [27], [28], and so on.

Particularly, if properly designed, these 1-D PhC nanobeam cavities can possess both ultra-high quality factor (Q) and ultra-small mode volume (V). This promising combination allows the enhancement of light-matter interactions, which makes them perfectly suitable for laboratory-on-a-chip applications, such as single particle detection, chemical, or bio-sensing [29]–[38].

However, sensitivities (S) and quality factors (Q) have been tradeoffs in label-free optical resonator sensors, and optical geometry that maximizes both factors is under active development. For example, Wang *et al.* demonstrated large sensitivity (S) of 900 nm/RIU in a slot double-beam waveguides/cavities. However, Q-factor was limited to 700, and the figure of merit (FOM) was ∼400 [32]. (Here, the FOM is defined as the resonance shift upon a change in the refractive index of the dielectric surrounding normalized by the resonance linewidth [39].) Lai *et al.* demonstrated photonic crystal sensors with high Q-factors ∼7000. However, sensitivity (S) was limited to ∼60 nm/RIU (refractive index unit), and FOM was ∼300 [33]. In order to overcome the trade-offs mentioned above and achieve ultrahigh S and Q-factor simultaneously, we theoretically and experimentally demonstrated a label-free sensor based on nanoslotted parallel quadrabeam photonic crystal cavity (NPQC) in our previous works [35], [36], where a theoretical (experimental) demonstration of sensitivity (S) of ∼800 nm/RIU (451 nm/RIU), and Q-factor of ∼10^7 (7015) at telecom wavelength range. This features FOM of > 2000, more than one order of magnitude improvement over previous photonic crystal sensors. However, the mode volume of the proposed PhC NPQC cavity in [35] and [36] is large ∼$10(\lambda/n)^3$, which leads to the large device footprint and low sensitivity when it is used to detect nanoparticles or proteins.

Recently, achieving small mode volumes is often pursued for nanoscale optical sensing applications. Small mode volume is also very important for reducing the footprint, energy requirements, and the molecular detection limit of optical nanosensors. A primary strategy for reducing the mode volume is introducing a dielectric discontinuity, or slot [40]–[46], which serves to simultaneously enhance the maximum field intensity and localize the maximum field to a region of lower refractive index [9]. Thus, in this paper, via combining the advantages between 1-D PhC nanobeam cavities and slot structures, we present a novel optical nanosensor based on the design of ultrahigh-Q and low mode volume single 1-D PhC slot nanobeam cavity (PhC-SNC). The basic structure is based on a slotted PhC single nanobeam cavity with a parabolically tapered air-holes. The slot effect provides strong field enhancement and subwavelength confinement to achieve high sensitivity simultaneously. With three-dimensional finite-difference-time-domain (3D-FDTD) method, we demonstrate that both an ultrahigh sensitivity (S) of 750.89 nm/RIU and a high Q factor of 2.67×10^7 in air at telecom wavelength range can be achieved simultaneously. The optimized FOM $> 10^7$ is obtained. In addition, with comparable S and Q factor, the proposed PhC-SNC geometry is exploited to achieve ultra-small mode volumes ∼$0.01(\lambda/n_{air})^3$, which is more than three orders of magnitude smaller than our previous works [35], [36]. Thus, this sensor device structure is potentially an ideal platform for realizing ultra-compact laboratory-on-a-chip applications.

The organization of this paper is as follows. In Section 2, we firstly describe the cavity design in detail, theoretical simulations methods and analog cavity characterizations demonstrating the performance of this architecture. The numerical simulations are used to analyze and confirm the suitability of PhC-SNC platform as a sensitive nanosensor. In Section 3, in order to illustrate the working of the proposed sensor device, we fill the sensing area with solutions possessing different refractive indices (RI). The sensitivity is determined by observing the shifts in the resonant wavelength ($\Delta\lambda$) of the resonators as a function of the variations in refractive index (Δn) in the region surrounding the cavity. Finally, in Section 4, we draw a brief conclusion.

2. Parabolic Radius-Modulated 1-D Photonic Crystal Slot Nanobeam Cavity (PhC-SNC) Design

The schematic of the single 1-D PhC-SNC described in this paper is shown in Fig. 1. It is formed by introducing a nano slot in the middle of a 1-D PhC single nanobeam cavity. The proposed 1-D PhC-SNC consists of air-holes ($n_{air} = 1.0$) in decreasing radii, etched into a silicon
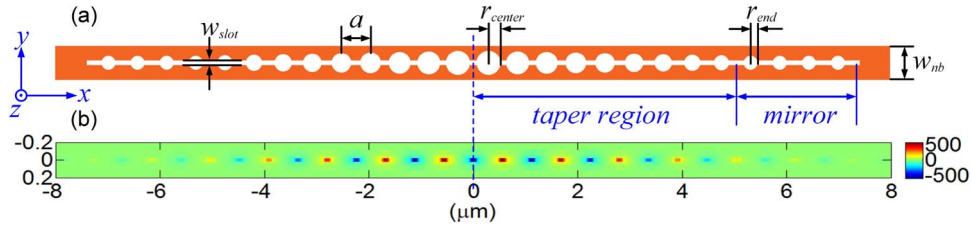
Fig. 1. (a) Schematics of the single 1-D PhC-SNC. The structure is symmetric with respect to its center (blue dashed line). a is the center-to-center distance between the gratings (periodicity); r_{center} and r_{end} are the radius of the gratings that are tapered parabolically from the center to both ends; w_{nb} and w_{slot} are the width of the 1-D PhC nanobeam and slot, respectively, and are kept constant. (b) 3D-FDTD simulation of the major field distribution profile (E_y) in the single 1-D PhC-SNC cavity. Here, the number of Gaussian mirror segments $i_{max} = 20$, with an additional 10 mirror segments on both ends of the Gaussian mirror (taper region). The calculated Q-factor is as high as 2.67×10^7, and the sensitivity S is 749.06 nm/RIU. Here, $a = 559$ nm, $w_{nb} = 650$ nm, $w_{slot} = 50$ nm, $h = 220$ nm, the hole radius is parabolically tapered from $r_{center} = 235$ nm in the center to $r_{end} = 203$ nm on both sides, i.e., $r(i) = r_{center} + (i-1)^2 (r_{end} - r_{center})/(i_{max} - 1)^2$ (i increases from 1 to i_{max}), $n_{si} = 3.46$, and $n_{air} = 1.0$. The unit of the x/y axis is micrometers.

($n_{si} = 3.46$) ridge waveguide with a width of 650 nm ($w_{nb} = 650$ nm). The thickness of the silicon ridge waveguide is $h = 220$ nm, and the periodicity of the air holes is $a = 559$ nm. The structure is symmetric with respect to the blue dashed line in Fig. 1. The radius of the center hole of the cavity is $r_{center} = 235$ nm. In the following discussion and simulation, we only consider the TE-polarized modes, as the TM band does not have a bandgap at small beam thickness [1], [12], [35]. To create a Gaussian mirror [12], [13], [47], the radius is parabolically tapered from $r_{center} = 235$ nm in the center to $r_{end} = 203$ nm on both sides, i.e., $r(i) = r_{center} + (i-1)^2 (r_{end} - r_{center})/(i_{max} - 1)^2$ (i increases from 1 to i_{max},), while the slot width (w_{slot}) and the nanobeam waveguide width (w_{nb}) keep unchanged. Here, the radius of air-hole gratings $r_{center} = 235$ nm and $r_{end} = 203$ nm, are chosen from the numerical band diagram simulations shown in Fig. 2(a) and (b), respectively. Fig. 2(a) shows the TE band diagrams of the single PhC slotted nanobeam with $r = 0.42a = 235$ nm (radius of the central hole) and $r = 0.36a = 203$ nm (radius of the edge hole). Here, in order to display the photonic bandgaps (PBGs) in TE band diagram clearly, we only draw the first bands above and below the PBGs (namely, the air mode and dielectric mode for each air hole radius [37]), which are below the light line. And the other band curves above the light line for each air hole radius are not displayed in the TE band diagram [Fig. 2(a)]. The three dimensional finite difference time domain (3D-FDTD) method with Bloch boundary conditions was utilized for the simulations. As expected, when the refractive index increases with the hole-radius decreasing, the band of the structure moves to lower frequency. So the band for the structure with $r = 235$ nm (red line with dots) is higher than the one for $r = 203$ nm (blue line with small triangles). Here, the green dot in Fig. 2(a) indicates the target resonance frequency ($\lambda_{res} \sim 1530$ nm) of the reported single 1-D PhC-SNC cavity. Fig. 2(b) shows the calculated mirror strength γ for different filling fraction ($f = \pi r^2/aw_{nb}$, r is the hole radius, and a is the lattice constant), where γ can be calculated by $\sqrt{(\omega_2 - \omega_1)^2/(\omega_2 + \omega_1)^2 - (\omega_{res} - \omega_0)^2/\omega_0^2}$, where ω_{res} is the proposed 1-D PhC-SNC target resonance, and ω_2, ω_1, and ω_0 are the air band edge, dielectric band edge, and midgap frequency of each segment, respectively [13]. As seen in Fig. 2(b), when filling fraction f is 0.3561 (namely, $r = 203$ nm), the maximum mirror strength is obtained [12], [13]. Thus the radius of the air-hole grating on both ends of the tapering section $r_{end} = 203$ nm is chosen to build 1-D PhC-SNC design.

In order to achieve a radiation-Q-limited cavity [37], we place 10 additional mirror segments at both edges of the Gaussian mirror, which have the same hole radius $r_{end} = 203$ nm. Through the 3D-FDTD simulation of the optimal structure mentioned above, a fundamental mode at $\lambda \sim 1530$ nm with a total calculated Q-factor as high as 2.67×10^7, and an mode volume of $V_{eff} \sim 0.01(\lambda/n_{air})^3$ is obtained, which is more than three orders of magnitude smaller than our
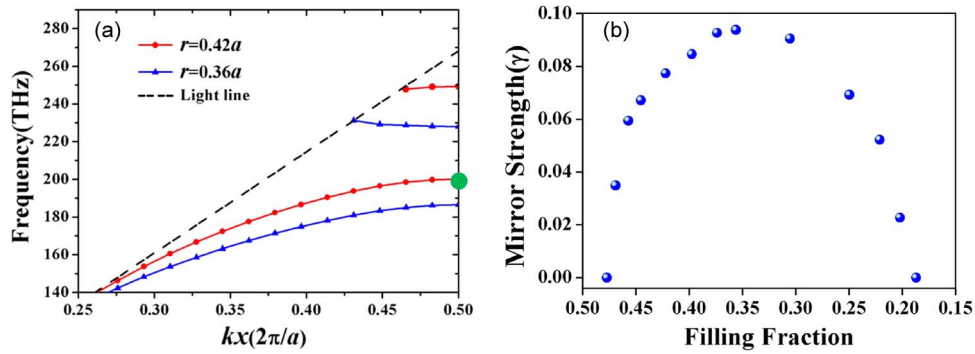
Fig. 2. (a) TE band diagram of the single PhC slotted nanobeam with $r = 0.42a = 235$ nm (red line with dots) and $r = 0.36a = 203$ nm (blue line with small triangles). In both cases, the width of the silicon ridge waveguide and the slot are kept constant at $w_{nb} = 650$ nm and $w_{slot} = 50$ nm, respectively. Besides, the periodicity of the air holes is $a = 559$ nm. The thickness of the silicon PhC nanobeam is $h = 220$ nm. The inset green dot indicates the target resonant frequency ($\lambda_{res} \sim 1530$ nm). (b) Mirror strength obtained by using 3D band-diagram simulation for different hole radii, while other structure parameters are kept the same as in (a).
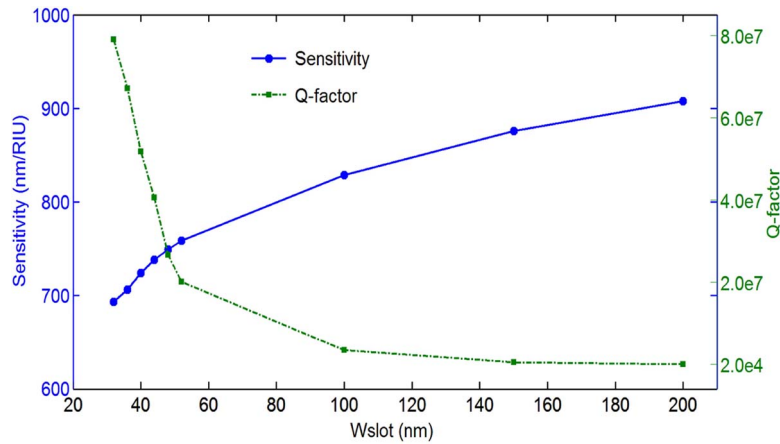

Fig. 3. Influence of the slot width (w_{slot}) on the Q-factors and sensitivities of single 1-D PhC-SNC sensor, while other structure parameters keep fixed.

previous works ($\sim 10(\lambda/n)^3$) [35], [36] (mode volume is defined as $V = \int dV \varepsilon |E|^2 / [\varepsilon |E|^2]_{max}$). Additionally, in comparison with recently reported designs with slot width quadratically tapered form an initial value to zero [38], our configuration offers almost two orders of magnitude improvement of $Q/V_{eff} \sim 2.68 \times 10^9$. Fig. 1(b) shows the top view of the major field distribution profile (E_y) in the structure mentioned above. It can be seen clearly that the majority of electric field is strongly localized in the slotted low-index area (namely, air region), indicating that a strong interaction between the analytes and the cavity mode can be achieved. Thus, the single 1-D PhC-SNC proposed in this paper is potentially an ideal platform for high-performance RI sensing.

Next, in order to discuss the sensing performances of the proposed 1-D PhC-SNC influenced by the width of the slot (w_{slot}), numerical 3D-FDTD simulations are calculated. Fig. 3 shows the Q-factors and the sensitivities varying as a function of the slot width. Here, the sensitivity is defined as the resonant wavelength shifts ($\Delta\lambda$) induced by the change of refractive index unit (Δn). As seen in Fig. 3, the cavity sensitivities increase as the slot width (w_{slot}) increased, while the Q-factors decrease exponentially by expanding the slot width. Moreover, it is worth mentioning that when the slot width $w_{slot} = 200$ nm, the sensitivity as high as $S = 907.6$ nm/RIU can be achieved, as shown in Fig. 3. Due to the trade-off between sensitivities (S) and quality factors

Fig. 4. Schematic diagram of the single 1-D PhC-SNC sensor obtained from 3D-FDTD optimization. The width of the silicon (Si) ridge waveguide and the slot are $w_{nb} = 650$ nm and $w_{slot} = 50$ nm, respectively. The periodicity of the holes is $a = 559$ nm, and the hole radius is parabolically tapered from $r_{center} = 235$ nm in the center to $r_{end} = 203$ nm on both sides with the number of gratings chosen to be i_{max}=10. The thickness of the silicon ridge waveguide is $h = 220$ nm for the entire device, which is symmetric with respect to its center. $n_{si} = 3.46$.

(Q) in label free optical sensors, in this paper we choose a trade-off value of the slot width $w_{slot} = 50$ nm to achieve ultra-high Q-factor ($> 10^7$) while keep an attractive high S (> 700 nm/ RIU) simultaneously. For the 1-D PhC-SNC cavity with slot width $w_{slot} = 50$ nm, $w_{nb} = 650$ nm, $a = 559$ nm, $h = 220$ nm, and the air-hole radius parabolically tapered from $r_{center} = 235$ nm in the center to $r_{end} = 203$ nm on either side, an ultra-high Q-factor of 2.67×10^7 at telecom wavelength range is obtained. Additionally, we also calculated S in the full cavity structure and obtained $S = 749.06$ nm/RIU. The optimized FOM is $\sim 1.31 \times 10^7$.

3. Simulated Transmission and RI Sensitivity of the Optimized 1-D PhC-SNC Sensor

Fig. 4 shows the schematic diagram of the single 1-D PhC-SNC sensor, which is based on the optimized single 1-D PhC-SNC cavity described above. As shown above, the structure consists of air-holes etched into a silicon ridge waveguide ($n_{si} = 3.46$) with width $w_{nb} = 650$ nm and thickness $h = 220$ nm. An air slot of $w_{slot} = 50$ nm is placed in the middle of structure to form the slotted photonic crystal single nanobeam cavity. The periodicity of the air-hole gratings is $a = 559$ nm. The radius of air holes ($n_{air} = 1.0$) is parabolically tapered from $r_{center} = 235$ nm in the center to $r_{end} = 203$ nm on both sides.

In order to save the simulation time of the transmission calculation, we use a high transmission but low Q-factor geometry. The number of gratings is chosen to be $i_{max} = 10$ and no additional mirror segments are placed outside of the Gaussian mirror region [35]–[37]. The total transmission spectrum of the single 1-D PhC-SNC sensor is shown in Fig. 5(a). A high Q-factor of $\sim 4.10 \times 10^3$ and near 70% transmission is obtained from the simulations. The resonant wavelength of the fundamental dielectric mode at 1529.92 nm is used for sensing, marked in Fig. 5(a), which is agree well with the target frequency ($\sim$1530 nm, green dot) obtained from bandgap simulation shown in Fig. 2(a). Here, the reasons why the resonant wavelength of the fundamental dielectric field mode at 1529.92 nm is selected for sensing evaluation and not other ones, as shown in Fig. 5(a), are as follows: 1) Compared with other modes, the fundamental dielectric mode can achieve larger Q-factor, resulting in larger FOM and lower detection limitation for practical sensing applications. 2) As seen in the transmission spectrum in Fig. 5(a), compared with the fundamental dielectric mode, other ones locate close to the band edge (namely the cutoff wavelength), resulting in the actual sensing detection difficult and inaccurate. Because during the sensing applications, as the refractive index increased, the modes will move towards longer wavelengths (red-shift) and exceeds the band edge.

To calculate the refractive index (RI) sensitivity S of the reported single 1-D PhC-SNC sensor, the transmission spectra of the fundamental mode used for sensing are calculated when the background refractive index changes from RI = 1.00 to RI = 1.18 ($\Delta n = 0.18$). As seen in Fig. 5(b), the resonant wavelength shift is $\Delta\lambda = 135.16$ nm. Therefore, the calculated RI sensitivity is $S = \Delta\lambda/\Delta n = 750.89$ nm/RIU. This agrees very well with our previous analysis obtained
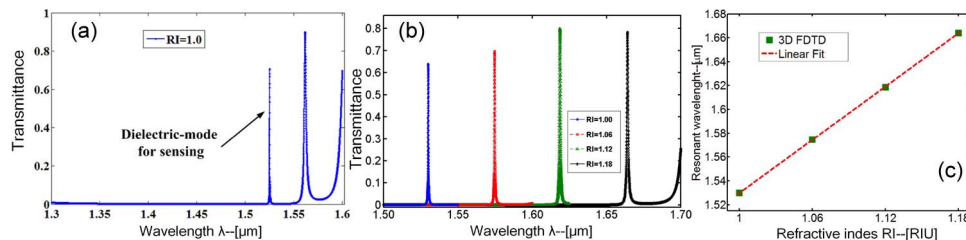
Fig. 5. (a) Transmission spectrum of the optimized single 1-D PhC-SNC sensor structure from 3D-FDTD simulation. The simulation consists of a PhC nanobeam waveguide with 10 tapered gratings in the taper region and no additional mirror segments. The background refractive index is set as RI $= 1.0$. A Q-factor of 4.10×10^3 and near 70% transmission is obtained. (b) Transmission spectra of the single 1-D PhC-SNC sensor when the background refractive index changes from RI $= 1.00$ to RI $= 1.18$. (c) Shift of the cavity resonant wavelength as a function of increased refractive index.

from the Q-factor simulation (749.06 nm/RIU). Herein, it is worth mentioning that, with a comparable ultrahigh sensitivity and Q-factor, the proposed 1-D PhC-SNC sensor in this paper possesses a much smaller mode volume than the previous sensors [35], [36]; thus, it is more attractive and promising in future optical high-density multiplexed gas sensing and nanophotonic integration. Moreover, compared with slotted multi-nanobeam cavities (e.g. double-nanobeam [32] and quadra-nanobeam [35]), the structures of the proposed single 1-D PhC-SNC are much more simple and easier to fabricate. In addition, the linear fit of the resonant wavelength shift with increased RI is shown in Fig. 5(c).

4. Conclusion

In summary, we have reported the design of an ultra-sensitive nanosensor based on a parabolic radius-modulated single 1-D photonic crystal slot nanobeam cavity (PhC-SNC) in silicon. With 3D-FDTD simulations, both ultra-high sensitivity $S > 750$ nm/RIU and ultra-high quality-factor $Q \sim 2.67 \times 10^7$ are achieved simultaneously. The highest refractive index sensitivity over 900 nm/RIU is also obtained. Moreover, the slotted geometry is exploited to provide strong light confinement and localized field enhancements, which results in an ultra-small mode volume $V_m \sim 0.01(\lambda/n_{\text{air}})^3$. With comparable high sensitivity and high Q-factor, the mode volume (V_m) of the proposed 1-D PhC-SNC sensor in this work is more than three orders of magnitude smaller than the previous works based on slotted parallel quadrabeam PhC cavities [35], [36]. Thus, the performance advantages of ultra-high sensitivity, ultra-high Q-factor, and ultra-small mode volume make the proposed single 1-D PhC-SNCs promising candidates for on-chip gas sensing arrays.

References

[1] J. D. Joannopoulos, S. G. Johnson, J. N. Winn, and R. D. Meade, *Photonic Crystals: Molding the Flow of Light*, 2nd ed. Princeton, NJ, USA: Princeton Univ. Press, 2008, p. 304.

[2] D. Yang, H. Tian, and Y. Ji, "Nanoscale photonic crystal sensor arrays on monolithic substrates using side-coupled resonant cavity arrays," *Opt. Exp.*, vol. 19, no. 21, pp. 20 023–20 034, 2011.

[3] A. Bera, M. Häyrinen, M. Kuittinen, S. Honkanen, and M. Roussey, "Parabolic opening in atomic layer deposited TiO2 nanobeam operating in visible wavelengths," *Opt. Exp.*, vol. 23, no. 11, pp. 14 973–14 980, 2015.

[4] Y. Li, C. Wang, and M. Loncar, "Design of nano-groove photonic crystal cavities in lithium niobate," *Opt. Lett.*, vol. 40, no. 12, pp. 2902–2905, 2015.

[5] A. Bazin, R. Raj, and F. Raineri, "Design of silica encapsulated high-Q photonic crystal nanobeam cavity," *J. Lightw. Technol.*, vol. 32, no. 5, pp. 952–958, Mar. 2014.

[6] M. J. Burek *et al.*, "High quality-factor optical nanocavities in bulk single-crystal diamond," *Nat. Commun.*, vol. 5, p. 5718, 2014.

[7] R. Miura, "Ultralow mode-volume photonic crystal nanobeam cavities for high-efficiency coupling to individual carbon nanotube emitters," *Nat. Commun.*, vol. 5, p. 5580, 2014.

[8] W. S. Fegadolli, J. E. B. Oliveira, V. R. Almeida, and A. Scherer, "Compact and low power consumption tunable photonic crystal nanobeam cavity," *Opt. Exp.*, vol. 21, no. 3, pp. 3861–3871, 2013.

[9] J. D. Ryckman and S. M. Weiss, "Low mode volume slotted photonic crystal single nanobeam cavity," *Appl. Phys. Lett.*, vol. 101, no. 7, 2012, Art. ID. 071104 .

[10] B. Desiatov, I. Goykhman, and U. Levy, "Parabolic tapered photonic crystal cavity in silicon," *Appl. Phys. Lett.*, vol. 100, no. 4, 2012, Art. ID. 041112.

[11] Q. Quan, I. B. Burgess, S. K. Y. Tang, D. L. Floyd, and M. Loncar, "High-Q, low index-contrast polymeric photonic crystal nanobeam cavities," *Opt. Exp.*, vol. 19, no. 22, pp. 22 191–22 197, 2011.

[12] Q. Quan and M. Loncar, "Deterministic design of wavelength scale, ultra-high Q photonic crystal nanobeam cavities," *Opt. Exp.*, vol. 19, no. 19, pp. 18 529–18 542, 2011.

[13] Q. Quan, P. B. Deotare, and M. Loncar, "Photonic crystal nanobeam cavity strongly coupled to the feeding waveguide," *Appl. Phys. Lett.*, vol. 96, no. 20, 2010, Art. ID. 203102.

[14] Y. Zhang, "Single-mode emission from Ge quantum dots in photonic crystal nanobeam cavity," *IEEE Photon. Technol. Lett.*, vol. 27, no. 9, pp. 1026–1029, May 2015.

[15] M. W. McCutcheon, D. E. Chang, Y. Zhang, M. D. Lukin, and M. Loncar, "Broadband frequency conversion and shaping of single photons emitted from a nonlinear cavity," *Opt. Exp.*, vol. 17, no. 25, pp. 22 689–22 703, 2009.

[16] S. Makino, Y. Ishizaka, K. Saitoh, and M. Koshiba, "Slow-light-enhanced nonlinear characteristics in slot waveguides composed of photonic crystal nanobeam cavities," *IEEE Photon. J.*, vol. 5, no. 2, Apr. 2013, Art. ID. 2700309.

[17] K. Rivoire, S. Buckley, and J. Vučković, "Multiply resonant photonic crystal nanocavities for nonlinear frequency conversion," *Opt. Exp.*, vol. 19, no. 22, pp. 22 198–22 207, 2011.

[18] H. Li and M. Li, "Optomechanical photon shuttling between photonic cavities," *Nat. Nanotechnol.*, vol. 9, pp. 913–919, 2014.

[19] J. Gomis-Bresco, "A one-dimensional optomechanical crystal with a complete phononic band gap," *Nat. Commun.*, vol. 5, Jul. 2014, Art. ID. 4452.

[20] M. Eichenfield, R. Camacho, J. Chan, K. J. Vahala, and O. Painter, "A picogram- and nanometre-scale photonic-crystal optomechanical cavity," *Nature*, vol. 459, pp. 550–555, May 2009.

[21] S. Lin, J. Hu, L. Kimerling, and K. Crozier, "Design of nanoslotted photonic crystal waveguide cavities for single nanoparticle trapping and detection," *Opt. Lett.*, vol. 34, no. 21, pp. 3451–3453, Nov. 2009.

[22] S. Mandal, X. Serey, and D. Erickson, "Nanomanipulation using silicon photonic crystal resonators," *Nano Lett.*, vol. 10, no. 1, pp. 99–104, 2010.

[23] J. Hendrickson, R. Soref, J. Sweet, and W. Buchwald, "Ultrasensitive silicon photonic-crystal nanobeam electro-optical modulator: Design and simulation," *Opt. Exp.*, vol. 22, no. 3, pp. 3271–3283, 2014.

[24] B. Schmidt, Q. Xu, J. Shakya, S. Manipatruni, and M. Lipson, "Compact electro-optic modulator on silicon-on-insulator substrates using cavities with ultra-small modal volumes," *Opt. Exp.*, vol. 15, no. 6, pp. 3140–3148, 2007.

[25] P. Lee, T. Lu, and L. Chiu, "Dielectric-band photonic crystal nanobeam lasers," *J. Lightw. Technol.*, vol. 31, no. 1, pp. 36–42, 2013.

[26] K. Jeong, "Electrically driven nanobeam laser," *Nat. Commun.*, vol. 4, 2013, Art. ID. 2822.

[27] X. Ge, Y. Shi, and S. He, "Ultra-compact channel drop filter based on photonic crystal nanobeam cavities utilizing a resonant tunneling effect," *Opt. Lett.*, vol. 39, no. 24, pp. 6973–6976, Dec. 2014.

[28] P. B. Deotare, "All optical reconfiguration of optomechanical filters," *Nat. Commun.*, vol. 3, p. 846, 2012.

[29] Q. Quan, "Single particle detection in CMOS compatible photonic crystal nanobeam cavities," *Opt. Exp.*, vol. 21, no. 26, pp. 32 225–32 233, 2013.

[30] F. Liang, N. Clarke, P. Patel, M. Loncar, and Q. Quan, "Scalable photonic crystal chips for high sensitivity protein detection," *Opt. Exp.*, vol. 21, no. 26, pp. 32 306–32 312, 2013.

[31] Q. Quan, "Ultrasensitive on-chip photonic crystal nanobeam sensor using optical bistability," in *Proc. Conf. QELS*, Baltimore, MD, USA, May 1, 2011, pp. 1–2.

[32] B. Wang, "Photonic crystal slot nanobeam slow light waveguides for refractive index sensing," *Appl. Phys. Lett.*, vol. 97, 2010, Art. ID. 151105.

[33] W. Lai, S. Chakravarty, Y. Zou, Y. Guo, and R. T. Chen, "Slow light enhanced sensitivity of resonance modes in photonic crystal biosensors," *Appl. Phys. Lett.*, vol. 102, no. 4, 2013, Art. ID. 041111.

[34] J. Zhou, "Refractive index sensing utilizing parallel tapered nano-slotted photonic crystal nanobeam cavities," *J. Opt. Soc. Amer. B, Opt. Phys.*, vol. 31, no. 8, pp. 1746–1752, 2014.

[35] D. Yang, H. Tian, Y. Ji, and Q. Quan, "Design of simultaneous high-Q and high-sensitivity photonic crystal refractive index sensors," *J. Opt. Soc. Amer. B, Opt. Phys.*, vol. 30, no. 8, pp. 2027–2031, 2013.

[36] D. Yang *et al.*, "High sensitivity and high Q-factor nanoslotted parallel quadrabeam photonic crystal cavity for real-time and label-free sensing," *Appl. Phys. Lett.*, vol. 105, no. 6, 2014, Art. ID. 063118.

[37] D. Yang, H. Tian, and Y. Ji, "High-Q and high-sensitivity width-modulated photonic crystal single nanobeam air-mode cavity for refractive index sensing," *Appl. Opt.*, vol. 54, no. 1, pp. 1–5, 2015.

[38] C. Wang, Q. Quan, S. Kita, Y. Li, and M. Lončar, "Single-nanoparticle detection with slot-mode photonic crystal cavities," *Appl. Phys. Lett.*, vol. 106, no. 26, 2015, Art. ID. 261105.

[39] L. J. Sherry, S. Chang, G. C. Schatz, and R. P. Van Duyne, "Localized surface plasmon resonance spectroscopy of single silver nanocubes," *Nano Lett.*, vol. 5, no. 10, pp. 2034–2038, Oct. 2005.

[40] V. R. Almeida, Q. Xu, C. A. Barrios, and M. Lipson, "Guiding and confining light in void nanostructure," *Opt. Lett.*, vol. 29, no. 11, pp. 1209–1211, 2004.

[41] J. T. Robinson, C. Manolatou, L. Chen, and M. Lipson, "Ultrasmall mode volumes in dielectric optical microcavities" *Phys. Rev. Lett.*, vol. 95, Sep. 2005, Art. ID. 143901.

[42] S. Kita, S. Hachuda, K. Nozaki, and T. Baba, "Nanoslot laser," *Appl. Phys. Lett.*, vol. 97, 2010, Art. ID. 161108.

[43] J. Jgersk, H. Zhang, Z. Diao, N. Le Thomas, and R. Houdre, "Refractive index sensing with an air-slot photonic crystal nanocavity," *Opt. Lett.*, vol. 35, no. 15, pp. 2523–2525, 2010.

[44] M. G. Scullion, A. Di Falco, and T. F. Krauss, "Slotted photonic crystal cavities with integrated microfluidics for bio-sensing applications," *Biosensors Bioelectronics*, vol. 27, no. 1, pp. 101–105, Sep. 2011.

[45] J. D. Ryckman and S. M. Weiss, "Localized field enhancement in guided and defect modes of a periodic slot wave-guide," *IEEE Photon. J.*, vol. 3, no. 6, pp. 986–995, Dec. 2011.

[46] P. Xu, K. Yao, J. Zheng, X. Guan, and Y. Shi, "Slotted photonic crystal nanobeam cavity with parabolic modulated width stack for refractive index sensing," *Opt. Exp.*, vol. 21, no. 22, pp. 26 908–26 913, Nov. 2013.

[47] P. B. Deotare, M. W. McCutchen, I. W. Frank, M. Khan, and M. Lončar, "High quality factor photonic crystal nano-beam cavities," *Appl. Phys. Lett.*, vol. 94, 2009, Art. ID. 121106.